PNAS RESEARCH ARTICLE | EARTH, ATMOSPHERIC, AND PLANETARY SCIENCES

Variable carbon isotope fractionation of photosynthetic communities over depth in an open-ocean euphotic zone

Lillian C. Henderson[a,1], Fabian Wittmers[b,c], Craig A. Carlson[d], Alexandra Z. Worden[b], and Hilary G. Close[a]

Edited by Akkihebbal Ravishankara, Colorado State University, Fort Collins, CO; received April 2, 2023; accepted January 3, 2024

Marine particulate organic carbon (POC) contributes to carbon export, food webs, and sediments, but uncertainties remain in its origins. Globally, variations in stable carbon isotope ratios ($\delta^{13}C$ values) of POC between the upper and lower euphotic zones (LEZ) indicate either varying aspects of photosynthetic communities or degradative alteration of POC. During summertime in the subtropical north Atlantic Ocean, we find that $\delta^{13}C$ values of the photosynthetic product phytol decreased by 6.3‰ and photosynthetic carbon isotope fractionation (ε_p) increased by 5.6‰ between the surface and the LEZ—variation as large as that found in the geologic record during major carbon cycle perturbations, but here reflecting vertical variation in $\delta^{13}C$ values of photosynthetic communities. We find that simultaneous variations in light intensity and phytoplankton community composition over depth may be important factors not fully accounted for in common models of photosynthetic carbon isotope fractionation. Using additional isotopic and cell count data, we estimate that photosynthetic and non-photosynthetic material (heterotrophs or detritus) contribute relatively constant proportions of POC throughout the euphotic zone but are isotopically more distinct in the LEZ. As a result, the large vertical differences in ε_p result in significant, but smaller, differences in the $\delta^{13}C$ values of total POC across the same depths (2.7‰). Vertical structuring of photosynthetic communities and export potential from the LEZ may vary across current and past ocean ecosystems; thus, LEZ photosynthesis may influence the exported and/or sedimentary $\delta^{13}C$ values of both phytol and total organic carbon and affect interpretations of ε_p over geologic time.

photosynthesis | carbon isotopes | ocean carbon cycle

Significance

The stable isotope ratio of carbon ($^{13}C/^{12}C$ or $\delta^{13}C$ value) in marine phytoplankton has been studied as an indicator of seawater carbon dioxide concentrations, growth rates, and community composition. Previous work focused on the ocean surface, but photosynthetic life extends deeper in open ocean environments. In the natural environment with native assemblages of phytoplankton, we find that the $\delta^{13}C$ values of deeper, low-light phytoplankton are lower than those at the surface. Sunlight intensity or small-cell community composition may drive this pattern at our open ocean site. The isotopic signature of low-light photosynthesis observed in the subtropical North Atlantic may be present in open ocean environments globally and thus may impact the interpretation of carbon isotopes broadly.

The dynamics of particulate organic carbon (POC) are a key variable of the marine carbon cycle. Importantly, POC supports the carbon and energy demands of marine food webs, but the portion that escapes remineralization can sink or otherwise be exported from the euphotic zone to the deep ocean via the biological carbon pump. Yet the definition of POC is purely operational: all combustible carbon captured on a glass or quartz filter—typically 0.7 or 1.0-μm pore size—after the removal of carbonates. Hence, POC encompasses not just non-living material, such as zooplankton molts and fecal pellets, nonviable cells, cell envelopes, aggregates, and terrigenous or advected POC, but also a diverse mixture of living protists, bacteria, and archaea (1). This broad definition and the combined collection of many types of organic matter hinder knowledge of the chemical and isotopic composition of individual components of POC, including original photosynthetic sources, relative quantities of autotrophic and heterotrophic biomass, the relative importance of different pathways of degradation, and dominant mechanisms of carbon export. Therefore, characterizing the sources and alteration pathways of organic particles in the water column is vital to a mechanistic understanding of ocean carbon cycling.

Stable carbon isotope ratios of POC ($\delta^{13}C_{POC}$) are one of the few properties that capture the whole of this diverse pool, and these values are affected by both production and degradation. Large-scale variations (10‰) in $\delta^{13}C_{POC}$ values across latitude are well recognized as resulting from primary producers in the mixed layer of the global ocean (2). More recently, a global data compilation of $\delta^{13}C_{POC}$ values from the open ocean showed significantly lower $\delta^{13}C_{POC}$ values in the lower euphotic zone (LEZ) compared to the upper euphotic zone (UEZ), with vertical variations in $\delta^{13}C_{POC}$ values of up to 6‰ in some locations (3). While $\delta^{13}C_{CO2}$ values are also lower in the LEZ vs. the near-surface, the magnitude of this difference in CO_2, as the photosynthetic substrate, [<1‰ on average; (4)] is not large enough to account for the observed variations in $\delta^{13}C_{POC}$ values. Failure to account for variability in $\delta^{13}C_{POC}$ values over depth can lead to inaccurate calculations where $\delta^{13}C_{POC}$ values are used as end-members, such as in food web studies, mixing models, carbon export and sedimentary studies, and carbon cycle models (5–8). Better understanding these vertical patterns in $\delta^{13}C_{POC}$ values and their drivers in nature, in this

Author contributions: L.C.H., C.A.C., and H.G.C. designed research; L.C.H., F.W., C.A.C., A.Z.W., and H.G.C. performed research; L.C.H., F.W., and H.G.C. analyzed data; and L.C.H., F.W., C.A.C., A.Z.W., and H.G.C. wrote the paper.

The authors declare no competing interest.

This article is a PNAS Direct Submission.

[1]To whom correspondence may be addressed. Email: lillian.henderson@earth.miami.edu.

This article contains supporting information online at https://www.pnas.org/lookup/suppl/doi:10.1073/pnas.2304613121/-/DCSupplemental.

Published February 26, 2024.

case, the open ocean euphotic zone, provides essential information about overall organic matter dynamics and thus context for the studies that rely on these data.

Despite numerous potential photosynthetic and degradative drivers, there is currently no consensus as to the mechanism responsible for relatively low $\delta^{13}C_{POC}$ values in the LEZ (3). Previous studies have analyzed $\delta^{13}C$ values of the ubiquitous photosynthetic pigment of phytoplankton, chlorophyll-*a*, or its side chain, phytol, as proxies for photosynthetic biomass (9–12). Some studies evaluated photosynthetic carbon isotope composition in the upper few meters of the water column and focused on variations between sites, while others focused largely on cultured isolates; however, to date, no study has systematically examined vertical variations in the water column.

Given the recent observations of Close and Henderson (3), we designed a study to specifically address the mechanism that drives the low $\delta^{13}C_{POC}$ values in the LEZ. Here, we sampled POC during summertime conditions (mixed layer depth 18 m) at the Bermuda Atlantic Time-series Study (BATS) site located in the seasonally oligotrophic North Atlantic open ocean (*SI Appendix*, Fig. S1). The average euphotic zone depth, defined as 0.1% surface irradiance (~1 to 1.9 μE m^{-2} s^{-1}), during the main study period (July 3 to 6, 2018) was 136 ± 11 m. For simplicity, we define the UEZ as 0 to 90 m (100 to 1% incident irradiance) and the LEZ as 90 to 136 m (1 to 0.1% incident irradiance). A vertical carbon isotope pattern in POC has been observed within the euphotic zone at this site (13) and is representative of oligotrophic environments that make up the majority of the ocean area and may expand in the future due to rising temperatures (14). We isolated the carbon isotope signatures of the in situ photosynthetic community by conducting compound-specific isotope analysis on phytol cleaved from intact polar lipids (chlorophyll, proxy for the photosynthetic community). We compare isotopic signatures of the in situ photosynthetic community with those of total POC, as well as environmental variables, phytoplankton community composition, and particle trophic position to identify drivers of low $\delta^{13}C$ values in the LEZ and better understand the particulate organic matter (POM) composition. We examine how the dynamics of autotrophic, heterotrophic, and degraded POM in the UEZ and the LEZ produce $\delta^{13}C_{POC}$ differences that are smaller than underlying isotopic variations in the photosynthetic community; thus, global vertical patterns in $\delta^{13}C_{POC}$ values may be driven by much larger underlying variations in the $\delta^{13}C$ values of photosynthetic biomass, reflected in phytol.

Results and Discussion

Evidence for Low $\delta^{13}C$ Values of Photoautotrophs in the LEZ. Results of our carbon isotopic analysis of phytol, a proxy for the integrated photosynthetic community, suggest that photosynthetic community biomass is responsible for vertical variations in $\delta^{13}C_{POC}$ values across the euphotic zone. The $\delta^{13}C$ values of phytol ($\delta^{13}C_{phytol}$) cleaved from intact polar lipids decreased by 6.3‰ between the UEZ and the LEZ in a 1.2- to 6-μm particle size fraction, while the $\delta^{13}C$ values of bulk POC ($\delta^{13}C_{POC}$) and total hydrolyzable amino acids (THAA; $\delta^{13}C_{THAA}$) in this size fraction decreased by 2.7‰ and 2.9‰, respectively, over the same depth range (Fig. 1*A*). We examined multiple size fractions of particles (0.3 to 1.2, 1.2 to 6, 6 to 20, >20-μm) but focus primarily on the 1.2- to 6-μm size fraction in this study because it contained the majority of total POC (69 ± 5%, n = 7) and most of the photosynthetic biomass during the sampling period at the BATS site. On average, 22 ± 2% (n = 7) of total POC was captured in the 0.3- to 1.2-μm size fraction, and measured phytol concentrations were 6 to 11% of those in the 1.2- to 6-μm size fraction at the same depths (*SI Appendix*, Table S1); $\delta^{13}C_{phytol}$ values of 0.3- to 1.2-μm particles also decreased from the near-surface to the LEZ (3.0‰; *SI Appendix*, Fig. S2). Vertical variations in overall $\delta^{13}C_{POC}$ values over the euphotic zone were similar during our main sampling period (July 2018) and in non-size fractionated POC we measured in August and November 2021, despite variations in the depths of the mixed layer and the deep chlorophyll maximum during these different sampling periods (*Materials and Methods* and *SI Appendix*, Fig. S3 and SI 5).

We used our measured $\delta^{13}C_{phytol}$ values to estimate the $\delta^{13}C$ value of photosynthetic biomass ($\delta^{13}C_p$) and, along with the $\delta^{13}C$ value of CO_2, the carbon isotopic fractionation expressed during photosynthetic carbon fixation (ε_p). Previous studies have also used the values of $\delta^{13}C_{phytol}$ as a proxy for those of $\delta^{13}C_p$ (9–11, 18), by assuming a constant offset between $\delta^{13}C_{phytol}$ and $\delta^{13}C_p$ values, $\Delta\delta^{13}C_{p\text{-}phytol}$, i.e.,

$$\delta^{13}C_p = \delta^{13}C_{phytol} + \Delta\delta^{13}C_{p-phytol}. \quad [1]$$

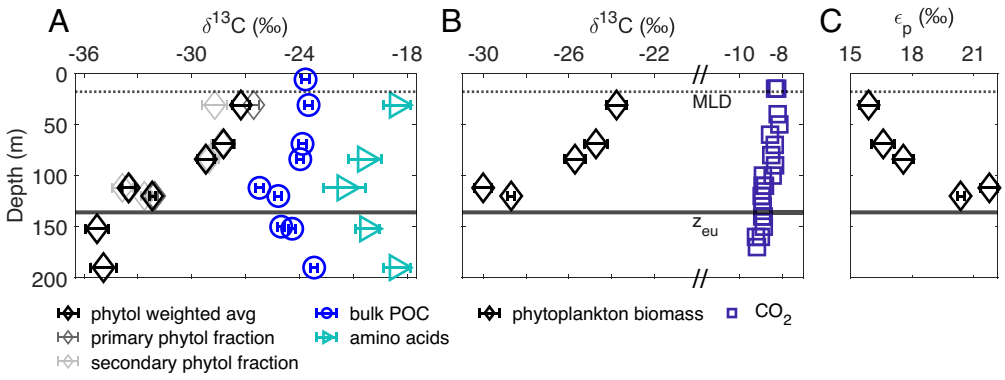

Fig. 1. (*A*) Measured $\delta^{13}C$ values of bulk POC, phytol from intact chlorophyll, and THAA (Eq. **3**, *Materials and Methods*). Primary phytol fraction refers to phytol cleaved from the intact polar lipid fraction, while secondary phytol fraction refers to phytol from the small amount of polar lipids that were recovered in the sterol fraction (*SI Appendix*, Table S1). The solid line marks euphotic zone depth at 0.1% surface irradiance (z_{eu}). $\delta^{13}C$ values are reported relative to Vienna Pee Dee Belemnite (VPDB); error bars indicate analytical uncertainty or propagated analytical uncertainty (±1σ; see *Materials and Methods*). Average $\delta^{13}C_{THAA}$ values were calculated as in ref. 15. (*B*) Calculated $\delta^{13}C$ values of phytoplankton biomass ($\delta^{13}C_p$) and $\delta^{13}C_{CO2}$. $\delta^{13}C_p$ was calculated from $\delta^{13}C$ values of phytol and a constant offset of 3.5‰ (16) between bulk biomass and phytol using Eq. **1**. $\delta^{13}C_{CO2}$ was calculated from the $\delta^{13}C$ value of total DIC as described in *SI Appendix*, SI 4.3. Symbols encompass analytical uncertainty. (*C*) ε_p values calculated from $\delta^{13}C_p$ and $\delta^{13}C_{CO2}$ values as in ref. 17 using Eq. **2**.

Isoprenoid lipids such as phytol generally have $\delta^{13}C$ values about 3.5 to 4‰ more negative than bulk biomass (16). While some discrepancies were found in batch vs. continuous cultures of phytoplankton (19), a recent compilation of culture data found a relatively narrow range of $\Delta\delta^{13}C_{p\text{-}phytol}$ across a variety of phytoplankton species [3.5 ± 1.3‰; (16)]. Previous studies have assumed $\Delta\delta^{13}C_{p\text{-}phytol}$ of 4‰ to calculate algal biomass $\delta^{13}C$ values (20, 21), and some have used this approach to infer whether environmental POM is composed mainly of algal biomass (9).

Using Eq. **1** with a literature mean $\Delta\delta^{13}C_{p\text{-}phytol}$ of 3.5‰, we found decreasing values of $\delta^{13}C_p$ with increasing depth (Fig. 1*B*). We also examined the possibility that $\Delta\delta^{13}C_{p\text{-}phytol}$ could vary with depth, thereby influencing values of $\delta^{13}C_{phytol}$ and the assumed relationship with values of $\delta^{13}C_p$. Testing a range of $\Delta\delta^{13}C_{p\text{-}phytol}$ from 2.2 to 4.8‰ [3.5‰ ± 1σ; (16)], a vertical decrease in $\delta^{13}C_p$ values remains apparent (*SI Appendix*, Fig. S4 and SI 2.1). Carbon:chlorophyll ratios also vary with photoacclimation across the euphotic zone (22); however, we calculate that the chlorophyll content, as a portion of the whole cell, is not large enough to affect values of $\delta^{13}C_p$ (*SI Appendix*, SI 2.1). We, therefore, interpret the decrease in $\delta^{13}C_{phytol}$ values over depth as an indication of a parallel decrease in the $\delta^{13}C$ value of whole photosynthetic biomass, i.e., $\delta^{13}C_p$. Cellular $\delta^{13}C_p$ values are a product of the $\delta^{13}C$ value of the photosynthetic substrate (i.e., $\delta^{13}C_{CO2}$) and the expressed carbon isotope fractionation associated with carbon fixation (ε_p). We calculate ε_p from $\delta^{13}C_p$ (Eq. **1**) and $\delta^{13}C_{CO2}$ values [Fig. 1*B* and *SI Appendix*, SI 4.3; (17)]:

$$\varepsilon_p = \frac{\delta^{13}C_{CO2} - \delta^{13}C_p}{1 + \left(\frac{\delta^{13}C_p}{1000}\right)}. \quad [2]$$

We determined that the whole-community ε_p increased by 5.6‰ from the UEZ to the LEZ in the 1.2- to 6-μm size fraction, with larger ε_p resulting in lower values of $\delta^{13}C_p$ in the LEZ (Fig. 1 *B* and *C*). The $\delta^{13}C_{CO2}$ values decreased by ~0.6 to 0.8‰ from the UEZ to the LEZ in August and November 2021 (Fig. 1*B*); both the magnitude and vertical pattern of this variation are typical for open-ocean water columns (e.g., ref. 4) and are insufficient to account for our observed variations in $\delta^{13}C_{phytol}$ or $\delta^{13}C_{POC}$. Notably, this calculation assumes that CO_2 is in isotopic equilibrium with the total measured dissolved inorganic carbon pool, a standard assumption in the calculation of ε_p (17).

We intended to isolate the $\delta^{13}C$ signal of the living, in situ photosynthetic community from that of detrital organic matter in our particle samples. The chlorophyll molecule is labile and thus, when captured intact, represents living or recently living photosynthetic biomass, while free phytol may persist in detrital material. We used silica gel chromatography (*Materials and Methods*) to separate extracted lipids into three compound class fractions: intact polar lipids (including intact chlorophyll, our target molecule), sterols, and other alcohols (including free phytol). We analyzed all three compound class fractions and recovered phytol cleaved from the polar lipid fraction in all samples from the upper 200 m of the water column (*SI Appendix*, Table S1). A small proportion of the polar lipids were captured in the sterol fraction of some samples (*SI Appendix*, Table S1), but the $\delta^{13}C$ values of phytol cleaved from this fraction were statistically indistinguishable from the polar lipid fraction in most cases (Fig. 1*A*). We report the weighted average $\delta^{13}C_{phytol}$ values of these two fractions throughout the rest of the manuscript. Our measurement of phytol cleaved from intact polar lipids included phytol derived from all forms of chlorophyll with phytol side chains—including chlorophyll *a*, *b*, *d*, and *f*—and, therefore, integrated a greater diversity of the photosynthetic community than would analysis of a single intact pigment. Phytol cleaved from polar lipids may also include contributions from phaeophytin, the product of chlorophyll demetallation, though data from previous studies suggest that $\delta^{13}C$ values of phytol cleaved from intact polar lipids can be considered indicative of the in situ photosynthetic community regardless of the inclusion of phaeophytin (23). Other molecules can also include phytol side chains, but these would not be included in our analysis of the polar lipid fraction (*SI Appendix*, SI 1). We detected negligible amounts of free phytol in our samples (*SI Appendix*, SI 1).

Potential Environmental and Phytoplankton Community Drivers of Variations in ε_p with Depth in the Euphotic Zone. We found variations over depth in the euphotic zone at our site for several potential factors controlling expressed photosynthetic carbon isotope fractionation (ε_p), including DIC (dissolved inorganic carbon), CO_2, and nitrate concentrations, phytoplankton specific growth rates and community composition, and light availability (*SI Appendix*, Figs. S5 and S6); both ε_p and $\delta^{13}C_{phytol}$ were significantly correlated with all of these parameters (Fig. 2 and *SI Appendix*, Fig. S7 and Tables S2 and S3). The examination of photosynthetic carbon isotope fractionation in laboratory cultures has focused primarily on how individual taxa respond under varying light, CO_2 concentrations, and growth rates (e.g., refs. 24–28). In contrast, in the natural environment, phytoplankton community composition varies simultaneously with properties such as light intensity, DIC concentrations, and phytoplankton growth rates, complicating the interpretation of water column ε_p and $\delta^{13}C$ data in relation to existing understanding from culture. To determine which parameters may be most important in controlling ε_p and $\delta^{13}C$ values of phytoplankton in our water column data, we explored our ε_p data in the context of canonical diffusive models of photosynthetic carbon isotope fractionation.

Diffusive models use phytoplankton specific growth rates (μ), cellular surface area to volume ratios (SA/V), and CO_2 concentrations to model photosynthetic carbon isotope fractionation (24, 30–32). Culture studies found a negative linear relationship between ε_p and $\mu/[CO_2]$, with different slopes depending on the species (Fig. 3*A*), and a single linear relationship between ε_p and $\mu/[CO_2] * (SA/V)^{-1}$ (Fig. 3*B*). We calculated $[CO_2]$ from measured [DIC] (*SI Appendix*, SI 4.2 and 4.3) and estimated μ and SA/V from measured net primary production (NPP) and calculated phytoplankton biomass (via cell abundances and chlorophyll fluorescence; *Materials and Methods*; *SI Appendix*, SI 2.2 and 2.3) for our study site. Overall, our data fall within the range of values of $\mu/[CO_2]$ and $\mu/[CO_2] * (SA/V)^{-1}$ previously studied, but our calculated ε_p values for the BATS community appear to respond more strongly to variations in $\mu/[CO_2] * (SA/V)^{-1}$ than those compiled from cultured phytoplankton species (Fig. 3*B*). In contrast, data from a surface transect of diatom-dominated phytoplankton communities in the Southern Ocean resulted in relationships closer to existing cultures [(9); Fig. 3*B* and *SI Appendix*, Table S6]; this (9) was the only other environmental study that included the parameters necessary to contextualize the relationship between ε_p and $\mu/[CO_2] * (SA/V)^{-1}$ within the diffusional model.

In the analysis above, we adjusted all environmental data to account for differences in the photoperiod used in cultures vs. the natural environment, as suggested by Laws et al. [(30); *SI Appendix*, SI 2.4]. Notably, the canonical linear relationship reproduced in Fig. 3*B* derives from cultures that were not limited by light nor by photoperiod, and the Southern Ocean data (9) derive only

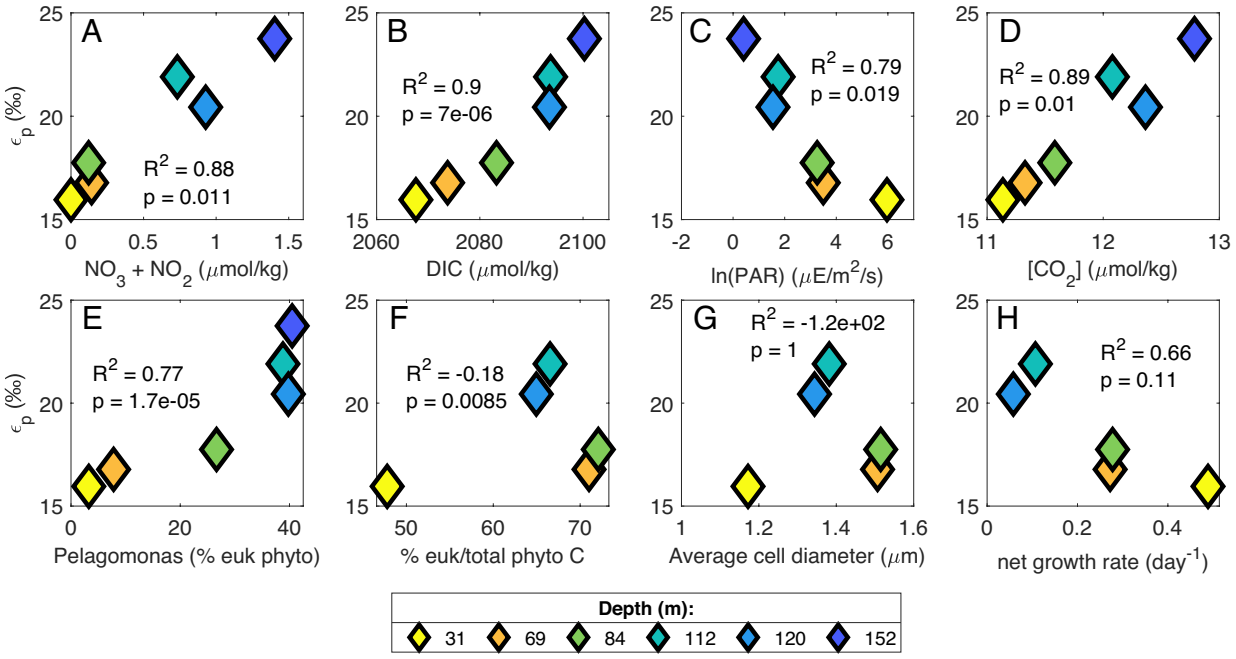

Fig. 2. Relationships between ε_p values of 1.2- to 6-μm particles and environmental parameters or phytoplankton community composition. Colors of symbols indicate depth of collection. R^2 and *P* values are based on orthogonal regression fit to data using MATLAB function linortfit2 (29). Data from 190 m have been omitted because that depth is below the euphotic zone and thus we did not calculate ε_p for that depth. (*A–D*) NO_3^-+NO_2^- concentration and photosynthetically available radiation (PAR) are from cruise AE1819 (July 2018). CO_2 concentration was calculated from measured DIC concentrations from AE2114 (August 2021). DIC concentration was averaged from BATS cruises June/July 2012-2019. (*E*) *Pelagomonas* relative abundance was calculated from size-fractionated v4 ASVs as a percentage of all plastid ASVs. (*F*) Percentage of total phytoplankton carbon that is composed of eukaryotic phytoplankton was estimated via measured cell abundances (*SI Appendix*, SI 2.3). (*G*) Phytoplankton growth rate was calculated from measured NPP (BATS cruises June/July 2018 to 2019 average) and phytoplankton biomass estimates (*SI Appendix*, SI 2.3). Panels (*F–H*) have no data at 152 m because the deepest depth of enumeration for cell abundances was 120 m.

from the near surface ocean (~100% surface irradiance), while our data include a wider range of light intensities (0.3 to 21.7% surface irradiance). Thus, we suggest the poor fit of existing models to our environmental data may be at least partially explained by light and/or phytoplankton community composition, as neither variable is included in diffusive models, both influence photosynthetic carbon isotope fractionation, and both were strongly correlated with ε_p and $\delta^{13}C_{phytol}$ values at our study site (Fig. 2 and *SI Appendix*, Fig. S7).

Light intensity can directly influence photosynthetic carbon isotope fractionation, specific growth rates, phytoplankton physiology, and the use of carbon concentrating mechanisms [CCMs; (25, 28, 30, 35–37)]. Light vs. nutrient limitation of growth can also impact the relative cellular allocation of resources into carbohydrates, proteins, and lipids (38). However, variations in relative abundances of macromolecules have been shown to influence $\delta^{13}C$ values of bulk phytoplankton biomass by only ~1‰ (39). Our data show increasing carbon isotope fractionation by an integrated phytoplankton community over increasing depth and decreasing light conditions across both measured size fractions (0.3 to 1.2 μm and 1.2 to 6 μm, *SI Appendix*, Fig. S2). Conversely, some studies targeting coccolithophorid algae have found either relatively constant or decreasing carbon isotopic fractionation with depth, as calculated from $\delta^{13}C$ values of alkenones (10, 40). Phelps et al. (28) recently included irradiance in addition to diffusional parameters in a model of photosynthetic carbon isotope fractionation by coccolithophores, finding a relationship between ε_p and irradiance that was opposite to what we find in this natural whole phytoplankton community, i.e., the irradiance model (28, 37) would predict decreasing ε_p with increasing depth. One diatom culture study also found lower ε_p in cultures with low light intensity compared to nitrate-limited cultures [(25); *SI Appendix*, Fig. S8]. However, the phytoplankton taxa used in these studies are not significant contributors to overall photosynthetic rates or biomass during summer stratified conditions at the BATS site (41–43).

Phytoplankton community composition is also well recognized as having an influence on photosynthetic carbon isotope fractionation, partly due to factors accounted for in diffusional models (growth rates and cell sizes), but also due to different photosynthetic enzymes [(37) and references therein], expression of CCMs, and other factors. Some culture studies suggest taxon-related (e.g., prokaryote vs. eukaryote) variations in the sensitivity of ε_p to varying CO_2 concentrations and growth rates (24), while others do not (34). We found no difference in the ratio of prokaryotes:eukaryotes between the UEZ and LEZ ($P > 0.05$, Kruskal–Wallis test) and no correlation between the fraction of phytoplankton biomass from eukaryotes and ε_p or $\delta^{13}C_{phytol}$ values (Fig. 2*F* and *SI Appendix*, Fig. S7*F*; $R^2 < 0$). However, we did observe correlations between the relative abundance of specific taxa and ε_p and $\delta^{13}C_{phytol}$ values. Namely, ε_p and $\delta^{13}C_{phytol}$ values were correlated with the relative abundance of *Pelagomonas calceolata* ($R^2 > 0.7$, $P < 0.001$; Fig. 2*E* and *SI Appendix*, Fig. S7*E*). In the LEZ, *Pelagomonas* comprised up to 40% of eukaryote plastid amplicons in the 1.2- to 6-μm size fraction compared to 3-7% in the upper 70 m (Fig. 2*E* and *SI Appendix*, SI 3.1 and 3.2). In the 0.3- to 1.2-μm size fraction, the relative contribution of *Prochlorococcus* and *Synechococcus* also varied significantly over depth (*SI Appendix*, SI 2.3). Total calculated biomass of *Prochlorococcus* increased from ~twofold less than *Synechococcus* at 20 m to ~30-fold greater by the deepest depth of enumeration (120 m). Thus, higher proportions of *Prochlorococcus* corresponded to lower $\delta^{13}C_{phytol}$ values and higher ε_p (*SI Appendix*, Figs. S9*B* and S10*B* and Tables S4 and S5). Analysis of whole seawater 16S rRNA gene amplicons also revealed a shift from high-light *Prochlorococcus* ecotypes in

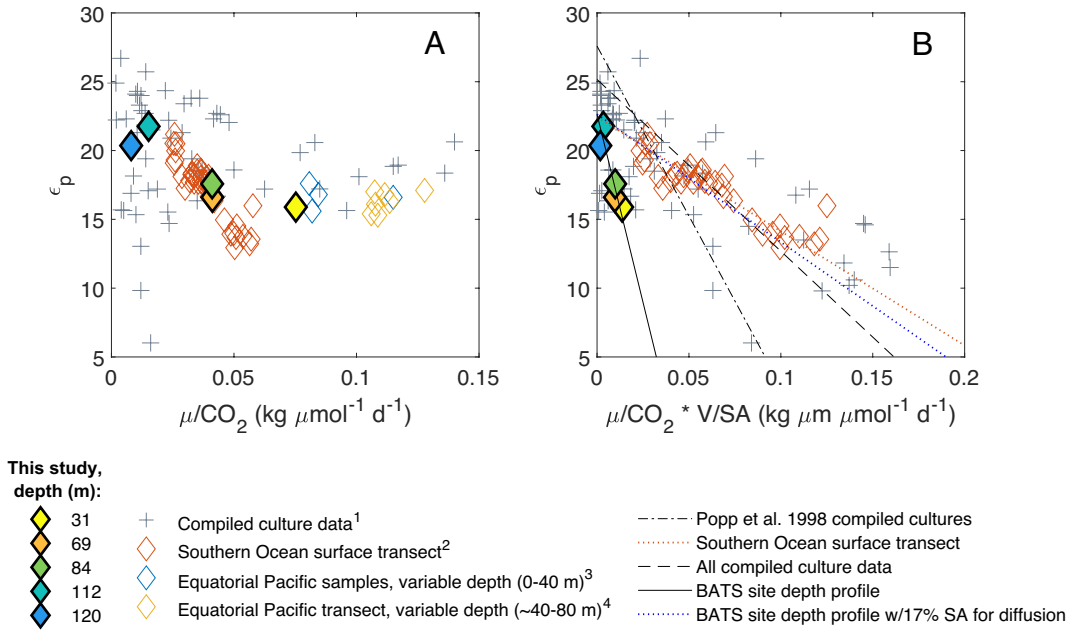

Fig. 3. Relationships between photosynthetic carbon isotope fractionation (ε_p) and (*A*) specific growth rate (μ) divided by CO_2 concentration, and (*B*) specific growth rate divided by CO_2 concentration, divided by the phytoplankton surface area (SA) to volume (V) ratio. For our data, specific growth rates were calculated via measured NPP and estimated phytoplankton biomass from measured cell abundances (*SI Appendix*, SI 2.3). Surface area to volume ratios were also estimated via cell abundances (*SI Appendix*, SI 2.3). Phytoplankton culture data are compiled from nitrate-limited chemostat cultures of *Alexandrium tamarense, Emiliania huxleyi, Phaeodactylum tricornutum, Porosira glacialis*, and *Synechococcus* strains CCMP838 and 7002. Environmental data are from this study [both panels, filled diamonds; (*B*) "BATS site depth profile" trend lines], surface samples in the Southern Ocean (both panels), and various depths in the equatorial Pacific (panel *A* only due to lack of cell size data). Mathematical relationships modeled after ref. 24; however, linear relationships here were fit using orthogonal linear regression [MATLAB function linortfit2; (29)], which results in a slope and intercept for compiled culture data different from those in ref. 24. Legend superscripts denote data from 1) refs. 24, 27, 31, 33, and 34; 2) ref. 9; 3) ref. 18; 4) ref. 30.

the UEZ to low-light ecotypes in the LEZ; this also correlated with changes in ε_p and $\delta^{13}C_{phytol}$ values in the 0.3- to 1.2-μm particles (*SI Appendix*, Figs. S9 *C* and *D* and S10 *C* and *D* and Tables S4 and S5).

Additional variables not included in diffusional models could be vital for understanding natural variations in ε_p, including the use of CCMs (44). All extant cyanobacteria and many marine eukaryotic phytoplankton have CCMs (45), and thus variable usage of CCMs over depth and changing community structure should be explored further. However, at the BATS site, our estimated μ/[CO_2] may be too low for the effect of CCMs on ε_p to be apparent, based on our estimates of the effective average radius of the photosynthetic communities [~1.5 μm, *SI Appendix*, Fig. S6*E* and SI 2.3; (31, 35, 44)]. Use of HCO_3^- as a photosynthetic substrate could affect $\delta^{13}C_p$ due to its $\delta^{13}C$ value being ~8 to 12‰ higher than CO_2 [depending on temperature; (46)]. However, this difference may be effectively canceled out by a 10.1‰ carbon isotopic fractionation during intracellular conversion of HCO_3^- to CO_2 by carbonic anhydrase, if HCO_3^- is present in excess (47). Further, a recent study suggests that temperature may be an important driver of $\delta^{13}C_{POC}$ values and ε_p, potentially due to effects on growth rates, usage of CCMs, or general phytoplankton physiology (48). Additionally, the proportion of carbon fixation resulting in products that are exuded from cells (dissolved primary production) can vary with phytoplankton cell sizes (49) and environmental conditions (50). Dissolved primary production is not captured as part of the isotopic mass balance considered in either culture or existing environmental studies of photosynthetic carbon isotope fractionation.

Finally, carbon isotopic fractionation by the phytoplankton community at our site appears more sensitive to SA/V than the relatively large phytoplankton examined in most culture studies (Fig. 3*B*). However, this pattern depends partially upon the assumption that 100% of the cell membrane is available for CO_2 diffusion. Using a cyanobacterial carbon isotope model, Hurley et al. (34) tested a range of 1 to 40% of the cellular surface area as available for CO_2 diffusion when fitting the model to experimental data. When we assigned a value of 17% of surface area allocated to CO_2 diffusion for the integrated phytoplankton communities at our site, our results aligned closely with the compiled culture data (Fig. 3*B* and *SI Appendix*, Table S6). Further, membrane permeability remains a relatively unconstrained variable in photosynthetic carbon isotope models (28), and thus could be an important consideration.

Comparison of our data with the diffusional model and culture study data suggests that variations in carbon supply and demand alone cannot explain the variations in ε_p and $\delta^{13}C_{phytol}$ we observed across the euphotic zone at the BATS site, despite observed relationships between ε_p and measured [CO_2] and growth rates (Fig. 2 *D* and *H*). Despite the omitted variables, the diffusional model has been included in biogeochemical models and has historically been the framework for reconstructing ancient atmospheric CO_2 concentrations from the $\delta^{13}C$ values of sedimentary organic matter (e.g., refs. 4, 6, and 17). Further synthesis of data from mixed communities and more varied cultures may offer insights on how to better interpret environmental ε_p data in the context of many simultaneously changing variables and elucidate the primary controls on $\delta^{13}C$ values of phytoplankton biomass in natural environments.

What Is POC Composed of in the LEZ? Relatively low $\delta^{13}C_{POC}$ values in the LEZ or upper mesopelagic have sometimes been assumed to indicate POC transformation during degradation (e.g., ref. 51), but our $\delta^{13}C_{phytol}$ data suggest that in situ photosynthetic community biomass drives vertical variations in $\delta^{13}C_{POC}$ values within the euphotic zone. We did not find a relationship between POC concentrations and $\delta^{13}C_{POC}$ values in our samples, further suggesting that decreases in $\delta^{13}C_{POC}$ values with depth in the euphotic zone are not controlled by POC degradation (*SI Appendix*, Fig. S11).

We observed decreases in the $\delta^{13}C$ values of phytol, amino acids, and bulk POC with increasing depth; however, the variations in $\delta^{13}C_{phytol}$ values were larger than those of the bulk POC and particulate amino acid pools (Fig. 1*A*). The $\delta^{13}C_{phytol}$ values represent only the primary biomass of the living, in situ photosynthetic community, while bulk POC and particulate amino acids integrate the $\delta^{13}C$ signals of living and dead autotrophic and heterotrophic biomass, heterotrophically altered POC, and other detritus. Thus, we suggest that the relatively low $\delta^{13}C$ signature of phytoplankton in the LEZ is partially diluted in the total POC and particulate amino acid pools by contributions from heterotrophic or non-living organic matter with relatively high $\delta^{13}C$ values.

Our estimates of phytoplankton biomass from cell counts and CTD fluorescence agree, suggesting that phytoplankton account for ~33 ± 12% of total POC on average within the euphotic zone (*SI Appendix*, Fig. S6*B* and SI 2.3). There was no significant difference between the UEZ and LEZ estimates ($P > 0.05$, Kruskal–Wallis test), similar to other findings at this site (52, 53). Because low-light phytoplankton biomass with relatively low $\delta^{13}C$ values is an important source of POC, the $\delta^{13}C$ values of integrated euphotic zone POC and photosynthetic biomass are, respectively, 0.4‰ and 1.1‰ lower than the surface values which are typically assumed to represent primary production. Thus, we conclude that it is not a greater proportion of non-phytoplankton POC (i.e., heterotrophic biomass or detrital POC) diluting the photosynthetic $\delta^{13}C$ signal in the LEZ, but rather that the difference in $\delta^{13}C$ values of phytoplankton and non-phytoplankton POC increases over depth. We used a mass balance calculation including the estimates of phytoplankton biomass above, the calculated $\delta^{13}C_p$, measured $\delta^{13}C_{POC}$, and measured POC concentrations to estimate the $\delta^{13}C$ value of non-phytoplankton POC (*SI Appendix*, SI 2.5 and Eq. **S1**). The difference between $\delta^{13}C$ values of phytoplankton biomass and non-phytoplankton POC was 4.6 to 6.5‰ in the LEZ and 0.4 to 3.1‰ in the UEZ (*SI Appendix*, Fig. S4*A*). In general, this points to POC pools with relatively homogeneous $\delta^{13}C$ values in the UEZ and relatively heterogeneous $\delta^{13}C$ values in the LEZ (Fig. 4).

We suggest that efficient community recycling in the nutrient-limited UEZ results in similar isotopic properties of autotrophs, heterotrophs, and detritus. This is supported by the low trophic position of ≤1, the value of primary producers, which we found in total POM in the surface mixed layer (Eq. **4**, *Materials and Methods*; *SI Appendix*, Fig. S12) despite the contribution of only ~20% autotrophic biomass to this total at this depth. In contrast, heterotrophic biomass and/or detrital POM are isotopically distinct from phytoplankton biomass in the LEZ (Fig. 4 and *SI Appendix*, Fig. S4*A*). A higher trophic position (1.5; Fig. 4 and *SI Appendix*, Fig. S12) of POM in the LEZ suggests this may be due to the introduction of metazoan waste products via disaggregation of large particles or an increasing reliance on amino acid catabolism by heterotrophic microbes (e.g., ref. 54). Overall, our isotopic data support a conceptual model of intense recycling in the nutrient-limited layer of a stratified water column and decreased reliance on the recycling of in situ primary production as nutrient concentrations increase with depth (Fig. 4).

Implications for Interpretation of $\delta^{13}C$ Data from Open-Ocean Water Columns. A statistically significant decrease in $\delta^{13}C_{POC}$ over depth in the euphotic zone has been observed in many stratified waters across the global ocean (3). The magnitude of this decrease in $\delta^{13}C_{POC}$ we observed at the BATS site (2.7‰) is a product of both variable photosynthetic carbon isotope fractionation and some dilution of the photosynthetic signal by detrital and heterotrophic organic matter within the total POC pool. Thus, the large variations in carbon isotope fractionation over depth that result in differences

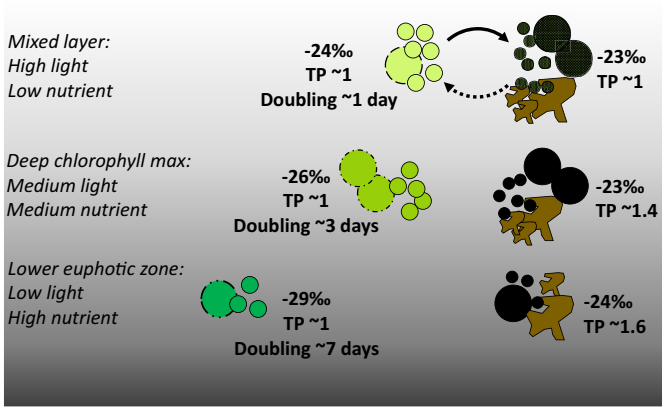

Fig. 4. Conceptual portrayal of quantities and isotopic characteristics (biomass $\delta^{13}C$ values and TP, trophic position) of phytoplankton and non-phytoplankton POM in a stratified, subtropical water column. Green circles represent phytoplankton, of which the phylogenies and chlorophyll content vary with depth; black circles represent heterotrophic microbes. Large and small circles indicate eukaryotes and prokaryotes, respectively. Brown shapes represent cell debris and other non-living detritus, which are grouped with heterotrophic cells in our calculations of non-phytoplankton isotopic properties. While we calculated the relative proportion of phytoplankton biomass and non-phytoplankton POM, the relative contribution of heterotrophic cells and non-living material to the latter is unknown currently. Relative specific growth rates of phytoplankton are indicated as doubling times [$\ln(2)*\mu^{-1}$]. Nearly all culture studies of carbon isotopic fractionation have simulated conditions similar to those of the mixed layer.

in $\delta^{13}C$ values of photosynthetic biomass may be beneficial to trace exported POC from its depth of origin. Further, the magnitude of vertical variation in $\delta^{13}C_{POC}$ values in the euphotic zone has been shown to vary across locations, with differences up to 6‰ (3). Thus, if a photosynthetic driver is also responsible in these other locations, the magnitude of variation in phytol may be even larger than observed here. Alternatively, similar variation in phytol and POC $\delta^{13}C$ values at a single site could indicate different organic matter dynamics from what we observed here. Better understanding the factors that control isotopic signatures of organic matter will allow for more accurate and thorough interpretation of $\delta^{13}C_{POC}$ values in natural environments.

Stratified, oligotrophic conditions, which already encompass approximately half of the global ocean area, are expanding and are expected to continue to do so with continued ocean warming (14). The data we present here and compiled elsewhere (3) identifies vertical carbon isotope patterns in the small particles (<53 μm) that dominate the contribution of total POC inventory in oligotrophic settings. Small particles can contribute to the sinking carbon flux through slow settling or aggregation/packaging (55, 56) or through non-sinking mechanisms such as mixed layer shoaling or eddy-driven subduction (57). Carbon export can originate from both the UEZ and the LEZ (e.g., ref. 58); for instance, zooplankton feeding and fecal packaging occur across the entire euphotic zone (e.g., ref. 59). Thus, variations in photosynthetic $\delta^{13}C$ values based on depth of origin should be considered in the interpretation of $\delta^{13}C$ values of sinking or sedimentary POM. For example, ε_p determined from $\delta^{13}C$ values of sedimentary phytol (phytane) can be used as a proxy for reconstructing past pCO_2 (e.g., ref. 16): variations of ≤7‰ have been interpreted to reflect twofold to fourfold variations in reconstructed pCO2 (11, 60, 61). Disregarding water column variations in $\delta^{13}C_{phytol}$ values (6.3‰ observed at the BATS site; this study) could lead to large errors in these calculations. Similar considerations apply to the interpretation of marine dietary sources using consumer $\delta^{13}C$ values in other stratified settings (e.g., refs. 5 and 62).

Conclusions

Here, we show that the in situ phytoplankton community is driving vertical variations in $\delta^{13}C_{POC}$ values within the euphotic zone in a stratified open-ocean setting. The observed $\delta^{13}C$ signal of the photosynthetic community, represented by >6‰ variations in $\delta^{13}C_{phytol}$ values, correlates with many factors known to influence photosynthetic carbon isotope fractionation, such as nutrient and DIC concentrations, light intensity, and various aspects of the photosynthetic community.

Much of the existing culture work addressing photosynthetic carbon isotopic fractionation has focused on phytoplankton isolates. However, in the natural environment with a mixed phytoplankton community, definitive explanations for variations in values of $\delta^{13}C_{phytol}$ and $\delta^{13}C_{POC}$ are complicated by simultaneous variations in multiple environmental parameters and/or phytoplankton community composition. In the context of existing models of photosynthetic carbon isotope fractionation, our observed variations in $\delta^{13}C_{phytol}$ values cannot be explained by diffusive controls alone. We hypothesize that light availability and photosynthetic community composition may be important in explaining part of the decreasing $\delta^{13}C_{phytol}$ and $\delta^{13}C_{POC}$ values observed over depth. Future work on photosynthetic carbon isotope fractionation with an emphasis on culturing more species, multiple strains of the same species, or mixed communities will aid in the interpretation of environmental data. Finding approaches to further combine and compare culture data with environmental community data will also aid in interpretation of environmental $\delta^{13}C$ data and may yield a better understanding of the factors dominating changes in photosynthetic carbon isotope fractionation in the natural environment.

Though the observed $\delta^{13}C_{POC}$ values are affected by those of the living photosynthetic community, the full magnitude of the photosynthetic carbon isotope signal is not expressed in the bulk POC and particulate amino acid $\delta^{13}C$ data, likely due to inputs of other types of POC (i.e., heterotrophic biomass and/or detritus). Our data here indicate that different types of POC in the LEZ may be more isotopically heterogeneous than those in the UEZ, leading to the dilution of the photosynthetic $\delta^{13}C$ signal despite similar fractional contributions from phytoplankton biomass in the UEZ and LEZ. More thorough characterization of different types of POM may further aid our interpretation of water column POM data as well as our interpretations of exported material collected in sediment traps and the sedimentary record.

Materials and Methods

Study Area and Environmental Conditions. The BATS site is located in the oligotrophic North Atlantic subtropical gyre, about 80 km southeast of Bermuda (31°40′N, 64°10′W; *SI Appendix*, Fig. S1). Water depth is >4,500 m. The site has a seasonally variable mixed layer depth, where the maximum winter mixed layer can be >300 m and summer mixed layer depths are typically less than 20 m (41).

Most samples were collected from the R/V *Atlantic Explorer* at the BATS site during July 3 to 6, 2018 (AE1819), with additional samples from August 5 to 8, 2021 (AE2114), and at nearby Hydrostation S during November 10 to 13, 2021 (AE2123). The BATS site and Hydrostation S are 60 km apart, with small seasonal differences between the two sites in the upper 1,500 m (63). Mixed layer depths during sampling were 18 ± 4 m, 18 ± 6 m, and 72 ± 5 m in July 2018, August 2021, and November 2021, respectively, calculated from potential density (64). The depth of the deep chlorophyll maximum was 90 m during our main sampling period.

Particle Samples for Geochemical and Taxonomic Analyses via In Situ Pumps. Size-fractionated particle samples were collected using McLane WTS-LV in situ pumps (McLane Research Laboratories, Inc.) in July 2018 (AE1819). Nine depths were sampled between the surface and 200 m, with high depth resolution within the euphotic zone. Most pumps were dual-flow pumps collecting water through two filter holders used, respectively, for 1) geochemical analyses and 2) taxonomic analyses. In some cases, individual, single-flow pumps were deployed for each type of analysis at depths 10 m apart. The sample depths were as follows (taxonomic single-flow pump depths in parentheses): 6, 28, 69 (79), 84, 112, 120, 150, and 190 (203) m. Total collected seawater volumes were 141 to 551 L and 54 to 367 L per sample for geochemical and taxonomic analyses, respectively, depending on the depth. Pumps were equipped with four 142 mm diameter filter tiers. The filter tiers were equipped as follows (from top to bottom): 1) 20-μm Nitex filter for both geochemical and taxonomic analyses, 2) 6-μm Nitex filter for geochemical analyses, 5-μm Osmonics polycarbonate filter for taxonomic analyses, 3) two stacked 1.2-μm glass fiber filters (GF/C) for geochemical analyses, 1.2-μm Millipore nitrocellulose mixed ester filter for taxonomic analyses, 4) two stacked 0.3-μm glass fiber filters (GF75) for geochemical analyses, 0.2-μm Supor polyethersulfone filter for taxonomic analyses. A 150-μm backing filter was placed beneath the filter(s) of interest on the first three tiers of all filter holders to ensure filter structural integrity. Nitex filters were acid and methanol washed beforehand, while glass fiber filters were pre-combusted (450 °C) for 4.5 h. Average flow rates were 1.9 to 3.1 and 0.7 to 2.0 L/min through the filters for geochemical and taxonomic analyses, respectively. After pump recovery, filter holders were drained with a weak vacuum to remove excess seawater from the filters. Filters for geochemical analysis were photographed, removed, and folded with clean forceps, stored in combusted foil, and transported and stored at −80 °C. Filters for taxonomic analysis were stored in sealed polyethylene bags at −80 °C.

Carbon Isotopes and Concentrations of Bulk POC. Glass fiber filters were split while frozen; sample proportions of wedge-shaped splits were determined by weight. Filter splits were then freeze-dried, and carbonates were removed via direct, dropwise addition of concentrated sulfurous acid to the filters, which were then dried at 60 °C overnight. Bulk POC concentration and isotope composition were measured using a Thermo Flash elemental analyzer coupled to a Conflo IV and MAT 253 Plus isotope ratio mass spectrometer (EA-IRMS, Thermo Scientific). Acetanilide and glycine standards of known carbon isotope composition (Arndt Schimmelmann, Indiana University) and mass were run alongside samples in order to calibrate isotope data and calculate sample concentrations. Analytical uncertainty in bulk $\delta^{13}C_{POC}$ values was 0.2‰. Values are reported relative to VPDB. Only results from the 1.2- to 6-μm and >20-μm size fractions are reported here, though the 0.3- to 1.2-μm size fraction was analyzed as well.

Extraction and Separation of Lipid Fractions. Chlorophyll was extracted from frozen or freeze-dried 1.2-μm GF/C and 0.3-μm GF75 filter splits as part of a total lipid extraction using a mixture of chilled methanol, dichloromethane, and milliQ water (2:1:0.8 v/v) (65, 66). Samples were sonicated for 5 min in an ice bath, vortexed/shaken vigorously for 5 min, and then cooled on ice in a −20 °C freezer for 5 min. This procedure was repeated 3 times. Additional dichloromethane and milliQ water were added to the sample to achieve a final methanol/dichloromethane/milliQ water ratio of 1:1:0.8. Samples were vortexed and centrifuged, and the lipid fraction was recovered. Lipid extracts were then filtered through a pre-combusted glass syringe packed with combusted glass wool to remove remaining filter material. The total lipid extract (TLE) was further purified via liquid–liquid extraction against salt water and dried under N_2. Lipid classes from each TLE were separated on silica gel (80 to 200 mesh, 60 Å, Avantor Performance Materials, LLC) mini-columns, with a 0.9 mL bed volume packed into pre-combusted 5-inch glass Pasteur pipettes with glass wool in the tip (67). Silica gel was fully activated, combusted at 450 °C and stored in a desiccator prior to use. Lipid classes were eluted with two bed volumes each of 100% hexane (non-polar fraction), 4:1 hexane/ethyl acetate (v/v) (alcohol fraction), 3:1 hexane/ethyl acetate (v/v) (sterol fraction), and ethyl acetate followed by methanol (2 bed volumes each, collected together; polar lipid fraction; e.g., ref. 68). Intact chlorophyll was expected to be recovered in the polar lipid fraction, but we examined the alcohol, sterol, and polar fractions for possible chlorophyll (cleaved phytol) and/or free phytol content. A portion of each fraction was aliquoted by volume and saponified (3:1 0.5 N KOH in methanol:milliQ water (v/v), 100 °C, 2 h) to cleave the phytol side chain from intact chlorophyll. Neutral lipids were obtained via liquid–liquid extraction from the basic mixtures using 4:1 hexane/dichloromethane mixture and 1 M NaCl in 3× dichloromethane-extracted milliQ water and concentrated at

40 °C using a Turbovap evaporator (Biotage, Inc.). Filter splits for carbon isotope analysis of phytol from intact polar lipids contained between 37 to 125 L and 46 to 99 L of seawater each for 1.2-μm GF/C and 0.3-μm GF75 filters, respectively. Free phytol was examined by analyzing unsaponified aliquots of the lipid fractions, i.e., without performing a cleavage reaction.

Carbon Isotopes and Concentrations of Phytol. Quantitative aliquots of both saponified and unsaponified alcohol, sterol, and polar lipid fractions were derivatized to trimethylsilyl (TMS) ethers using 1:1 pyridine/N,O-bis(trimethylsilyl) trifluoroacetamide (BSTFA) (v/v) (60 °C, 45 min). Both saponified and unsaponified TMS-derivatized samples were analyzed via gas chromatography–mass spectrometry (GC-MS; Agilent 6890N GC, 5973 MS) with a TG-5MS column (30 m × 0.25 mm, 0.25-μm film thickness; Thermo Scientific). Final prepared sample volumes were 5 to 16 μL. Samples were analyzed within the same day of derivatization and compared with phytol standards of known concentrations to calculate sample phytol concentrations. Chlorophyll concentrations were calculated from measured phytol concentrations by using the molecular weight of chlorophyll a. Contaminant alkanes were identified in some samples and in the procedural blank, but no phytol was detected in the blank. In samples containing contaminant alkanes, cleaved phytol was further purified via a second round of silica gel column chromatography, wherein cleaved phytol was recovered in the 3:1 hexane/ethyl acetate fraction.

Samples containing sufficient phytol were analyzed for stable carbon isotope composition via gas chromatography–isotope ratio mass spectrometry (GC-IRMS; Thermo Scientific Trace 1310 GC Isolink/ConFlo IV/MAT 253 Plus IRMS) equipped with a TG-5MS column (30 m × 0.25 mm, 0.25-μm film thickness; Thermo Scientific). A separate aliquot was derivatized for this purpose and analyzed on the same day of derivatization, as described for quantification via GC-MS. To improve GC-IRMS chromatography, the pyridine/BSTFA derivatization solution was evaporated to a small volume under N_2, and small volumes of hexane were added according to expected phytol concentrations. Due to the small volume of pyridine/BSTFA remaining, sample volumes were not exact, and phytol concentrations obtained from GC-IRMS analysis are considered semi-quantitative. Final prepared sample volumes were ~1.5 to 15 μL. Samples were injected via a splitless injector held at 220 °C, and the GC column temperature was held at 60 °C for 1 min, increased to 160 °C at 20 °C/min, increased to 300 °C at 13 °C/min, and then held constant at 300 °C for 5 min. The Thermo GC Isolink combustion interface was held at a constant temperature of 1,000 °C. Phytol standards of a known $\delta^{13}C$ value (measured via EA-IRMS) were derivatized alongside samples to account for isotope fractionation during the derivatization reaction as well as the $\delta^{13}C$ value of added derivative carbon. A mass balance calculation was used to correct for the added three derivative carbon atoms to the initial 20-carbon phytol molecule. Samples were analyzed with duplicate or triplicate injections where possible; for some samples, only a single injection was possible. 5 of 7 polar lipid fractions were measured in duplicate or triplicate; the samples at 152 and 190 m were only analyzed once due to limited sample. All measured sterol fractions were analyzed only once due to limited sample. For samples with duplicate or triplicate injections, error was propagated to include 1) uncertainty in the $\delta^{13}C$ value of the standard, 2) the replicate variability of the standard, and 3) the replicate variability of the sample. When only a single injection was possible, error was propagated the same way with an assumed sample SD of 0.38‰, the maximum daily SD of the phytol standard across all days where samples were analyzed. 7 samples in the 1.2- to 6-μm size fraction and 3 samples in the 0.3- to 1.2-μm size fraction were analyzed for $\delta^{13}C_{phytol}$ values; sample depths ranged from 31 to 190 m and 31 to 112 m for the 1.2- to 6- and 0.3- to 1.2-μm size fractions, respectively. Reported $\delta^{13}C_{phytol}$ data are the measured $\delta^{13}C_{phytol}$ values in the saponified polar lipid fraction or the weighted average of the saponified polar lipid and sterol fractions, where phytol was present in both. $\delta^{13}C$ values are reported relative to VPDB.

Amino Acid Analysis. Quantitative splits from 0.3-μm GF75 and 1.2-μm GF/C filters were freeze-dried, hydrolyzed, purified, derivatized, and analyzed for nitrogen and carbon isotope composition of individual amino acids via GC-IRMS as in ref. 69. Detailed methods are described in *SI Appendix*, SI 5. Filter splits contained between 28 to 127 L and 46 to 70 L for 1.2-μm GF/C and 0.3-μm GF75 filters, respectively.

$\delta^{13}C$ values of THAA ($\delta^{13}C_{THAA}$) were calculated as in ref. 15:

$$\delta^{13}C_{THAA} = \Sigma\left(\delta^{13}C_{AA} * \text{mol}\%_{AA}\right), \quad [3]$$

where $\delta^{13}C_{AA}$ and $\text{mol}\%_{AA}$ are the $\delta^{13}C$ value and the molar percentage contribution of each individual amino acid, respectively. $\delta^{13}C$ values are reported relative to VPDB. SD for each sample was calculated as the square root of the weighted average of variances of each individual amino acid.

We also report POM trophic position (TP) as calculated from measured $\delta^{15}N$ values of glutamic acid+glutamine (Glx) and phenylalanine (Phe) as in ref. 70:

$$TP = \left(\delta^{15}N_{Glx} - \delta^{15}N_{Phe} - 3.4\right)/7.6 + 1, \quad [4]$$

TP propagated uncertainty was calculated as in ref. 71.

Phytoplankton Community Characterization. DNA extraction and amplicon sequencing methods for size-fractionated particle samples collected for taxonomic analysis are described in *SI Appendix*, SI 3.1 and 3.2. Water samples were also collected and analyzed for whole seawater amplicon sequencing (*SI Appendix*, SI 3.3–3.5) and flow cytometry cell enumeration (*SI Appendix*, SI 2.2). Phytoplankton community biomass was estimated using multiple independent calculations: from chlorophyll to carbon ratios and measured CTD fluorescence (52, 53) and measured cell abundances via flow cytometry, previously measured cell diameters (42), and a biovolume to cellular carbon conversion factor (72, 73); methods are described in further detail in *SI Appendix*, SI 2.3. Average phytoplankton cell diameters and surface area to volume ratios were also estimated from measured cell abundances via flow cytometry and previously measured cell diameters (42). NPP data averaged from BATS cruises in June and July 2018 to 2019 was normalized to estimated in situ phytoplankton biomass to estimate average phytoplankton growth rates (*SI Appendix*, SI 2.3). Overall, specific growth rates derived from NPP measurements presented here are consistent with ^{14}C bicarbonate incubations as well as dilution experiments conducted in the Sargasso Sea (e.g., see ref. 74 and references therein).

Seawater Chemistry. Water samples were collected and analyzed for nitrate concentrations (*SI Appendix*, SI 4.1), DIC speciation, and DIC isotope composition (*SI Appendix*, SI 4.2). CO_2 concentrations were calculated from measured DIC and alkalinity concentrations using CO2SYS [(75); *SI Appendix*, SI 4.3]. DIC concentrations were also obtained for comparison from all BATS cruises in June and July, from 2012 to 2019 (available at http://bats.bios.edu/bats-data/). $\delta^{13}C_{CO2}$ values were calculated from measured $\delta^{13}C_{DIC}$ values [(32, 46); *SI Appendix*, SI 4.3], and ε_p values for the integrated phytoplankton community were calculated according to Eq. **2**.

Data, Materials, and Software Availability. All data in this manuscript have been deposited at the BIOS-SCOPE BCO-DMO page (76) (https://www.bco-dmo.org/project/826178).

ACKNOWLEDGMENTS. This work was funded by Simons Foundation International's BIOS-SCOPE program. We thank Jacqui Comstock and Shuting Liu for their rRNA amplicon analyses on size-fractionated particle samples, Luis Bolaños and Kevin Vergin for their rRNA amplicon analyses on whole-seawater samples, Kristin Bergauer and Camille Poirier for flow cytometry sample collection and data, respectively, the rest of the BIOS-SCOPE team for ancillary environmental data, Becky Garley and the Bates Lab for DIC/alkalinity analysis, Amel Saied and Peter Swart of the University of Miami Stable Isotope Laboratory for $\delta^{13}C_{DIC}$ analysis, the crew of the R/V *Atlantic Explorer*, Rachel Parsons and the BATS team for pre and post-cruise logistical support, Paul Wojtal and Albert Ortiz for their help with sample preparation and analysis, Sarah Hurley for helpful conversations, and two anonymous reviewers for comments that greatly improved the quality of the manuscript.

Author affiliations: [a]Department of Ocean Sciences, Rosenstiel School of Marine, Atmospheric, and Earth Science, University of Miami, Miami, FL 33149; [b]Josephine Bay Paul Center for Comparative Molecular Biology and Evolution, Marine Biological Laboratory, Woods Hole, MA 02543; [c]Faculty of Mathematics and Natural Sciences, Christian-Albrecht University of Kiel, Kiel SH 24118, Germany; and [d]Department of Ecology, Evolution, and Marine Biology/Marine Science Institute, University of California, Santa Barbara, CA 93106

1. J. J. Kharbush *et al.*, Particulate organic carbon deconstructed: Molecular and chemical composition of particulate organic carbon in the Ocean. *Front. Mar. Sci.* **7**, 518 (2020).
2. R. Goericke, B. Fry, Variations of marine plankton δ13C with latitude, temperature, and dissolved CO_2 in the world ocean. *Global Biogeochem. Cycles* **8**, 85–90 (1994).
3. H. G. Close, L. C. Henderson, Open-ocean minima in δ13C values of particulate organic carbon in the lower euphotic zone. *Front. Mar. Sci.* **7**, 540165 (2020).
4. A. Schmittner *et al.*, Biology and air–sea gas exchange controls on the distribution of carbon isotope ratios (δ13C) in the ocean. *Biogeosciences* **10**, 5793–5816 (2013).
5. B. Fry, S. C. Wainright, Diatom sources of 13C-rich carbon in marine food webs. *Mar. Ecol. Prog. Ser.* **76**, 149–157 (1991).
6. A. Tagliabue, L. Bopp, Towards understanding global variability in ocean carbon-13. *Global Biogeochem. Cycles* **22**, GB1025 (2008).
7. G. Luo *et al.*, Vertical δ13Corg gradients record changes in planktonic microbial community composition during the end-Permian mass extinction. *Palaeogeogr. Palaeoclimatol. Palaeoecol.* **396**, 119–131 (2014).
8. S. Magozzi, A. Yool, H. B. V. Zanden, M. B. Wunder, C. N. Trueman, Using ocean models to predict spatial and temporal variation in marine carbon isotopes. *Ecosphere* **8**, e01763 (2017).
9. B. N. Popp *et al.*, Controls on the carbon isotopic composition of southern ocean phytoplankton. *Global Biogeochem. Cycles* **13**, 827–843 (1999).
10. I. Tolosa *et al.*, Distribution of lipid biomarkers and carbon isotope fractionation in contrasting trophic environments of the South East Pacific. *Biogeosciences* **5**, 949–968 (2008).
11. C. R. Witkowski *et al.*, Validation of carbon isotope fractionation in algal lipids as a pCO_2 proxy using a natural CO_2 seep (Shikine Island, Japan). *Biogeosciences* **16**, 4451–4461 (2019).
12. J. P. Sachs, D. J. Repeta, R. Goericke, Nitrogen and carbon isotopic ratios of chlorophyll from marine phytoplankton. *Geochim. Cosmochim. Acta* **63**, 1431–1441 (1999).
13. R. Pedrosa-Pàmies, M. H. Conte, J. C. Weber, R. Johnson, Carbon cycling in the Sargasso Sea water column: Insights from lipid biomarkers in suspended particles. *Prog. Oceanogr.* **168**, 248–278 (2018).
14. J. J. Polovina, E. A. Howell, M. Abecassis, Ocean's least productive waters are expanding. *Geophys. Res. Lett.* **35**, L03618 (2008).
15. M. D. McCarthy, J. Lehman, R. Kudela, Compound-specific amino acid δ15N patterns in marine algae: Tracer potential for cyanobacterial vs. eukaryotic organic nitrogen sources in the ocean. *Geochim. Cosmochim. Acta* **103**, 104–120 (2013).
16. C. R. Witkowski, J. W. H. Weijers, B. Blais, S. Schouten, J. S. Sinninghe Damsté, Molecular fossils from phytoplankton reveal secular PCO_2 trend over the Phanerozoic. *Sci. Adv.* **4**, eaat4556 (2018).
17. K. H. Freeman, J. M. Hayes, Fractionation of carbon isotopes by phytoplankton and estimates of ancient CO_2 levels. *Global Biogeochem. Cycles* **6**, 185–198 (1992).
18. R. R. Bidigare *et al.*, Iron-stimulated changes in 13C fractionation and export by equatorial Pacific phytoplankton: Toward a paleogrowth rate proxy. *Paleoceanography* **14**, 589–595 (1999).
19. S. Schouten *et al.*, Biosynthetic effects on the stable carbon isotopic compositions of algal lipids: Implications for deciphering the carbon isotopic biomarker record. *Geochim. Cosmochim. Acta* **62**, 1397–1406 (1998).
20. R. D. Pancost, K. H. Freeman, S. G. Wakeham, C. Y. Robertson, Controls on carbon isotope fractionation by diatoms in the Peru upwelling region. *Geochim. Cosmochim. Acta* **61**, 4983–4991 (1997).
21. R. D. Pancost, K. H. Freeman, S. G. Wakeham, Controls on the carbon-isotope compositions of compounds in Peru surface waters. *Org. Geochem.* **30**, 319–340 (1999).
22. J. J. Cullen, Subsurface chlorophyll maximum layers: Enduring enigma or mystery solved? *Annu. Rev. Mar. Sci.* **7**, 207–239 (2015).
23. C. S. Yentsch, Distribution of chlorophyll and phaeophytin in the open ocean. *Deep Sea Res. Oceanogr. Abstr.* **12**, 653–666 (1965).
24. B. N. Popp *et al.*, Effect of phytoplankton cell geometry on carbon isotopic fractionation. *Geochim. Cosmochim. Acta* **62**, 69–77 (1998).
25. U. Riebesell, S. Burkhardt, A. Dauelsberg, B. Kroon, Carbon isotope fractionation by a marine diatom: Dependence on the growth-rate-limiting resource. *Mar. Ecol. Prog. Ser.* **193**, 295–303 (2000).
26. U. Riebesell, A. T. Revill, D. G. Holdsworth, J. K. Volkman, The effects of varying CO_2 concentration on lipid composition and carbon isotope fractionation in Emiliania huxleyi. *Geochim. Cosmochim. Acta* **64**, 4179–4192 (2000).
27. E. B. Wilkes, S. J. Carter, A. Pearson, CO_2-dependent carbon isotope fractionation in the dinoflagellate Alexandrium tamarense. *Geochim. Cosmochim. Acta* **212**, 48–61 (2017).
28. S. R. Phelps *et al.*, Carbon isotope fractionation in Noelaerhabdaceae algae in culture and a critical evaluation of the alkenone paleobarometer. *Geochem. Geophys. Geosyst.* **22**, e2021GC009657 (2021).
29. F. Carr, Orthogonal linear regression. MATLAB Central File Exchange (2023). https://www.mathworks.com/matlabcentral/fileexchange/16800-orthogonal-linear-regression (25 September 2023).
30. E. A. Laws, B. N. Popp, J. R. R. Bidigare, M. C. Kennicutt, S. A. Macko, Dependence of phytoplankton carbon isotopic composition on growth rate and $[CO_2]$aq: Theoretical considerations and experimental results. *Geochim. Cosmochim. Acta* **59**, 1131–1138 (1995).
31. E. A. Laws, R. R. Bidigare, B. N. Popp, Effect of growth rate and CO2 concentration on carbon isotopic fractionation by the marine diatom *Phaeodactylum tricornutum*. *Limnol. Oceanogr.* **42**, 1552–1560 (1997).
32. G. H. Rau, U. Riebesell, D. Wolf-Gladrow, A model of photosynthetic 13C fractionation by marine phytoplankton based on diffusive molecular CO2 uptake. *Mar. Ecol. Prog. Ser.* **133**, 275–285 (1996).
33. R. R. Bidigare *et al.*, Consistent fractionation of 13C in nature and in the laboratory: Growth-rate effects in some haptophyte algae. *Global Biogeochem. Cycles* **11**, 279–292 (1997).
34. S. J. Hurley, B. A. Wing, C. E. Jasper, N. C. Hill, J. C. Cameron, Carbon isotope evidence for the global physiology of Proterozoic cyanobacteria. *Sci. Adv.* **7**, eabc8998 (2021).
35. N. Cassar, E. A. Laws, B. N. Popp, Carbon isotopic fractionation by the marine diatom Phaeodactylum tricornutum under nutrient- and light-limited growth conditions. *Geochim. Cosmochim. Acta* **70**, 5323–5335 (2006).
36. N. Cassar, E. A. Laws, Potential contribution of β-carboxylases to photosynthetic carbon isotope fractionation in a marine diatom. *Phycologia* **46**, 307–314 (2007).
37. E. B. Wilkes, A. Pearson, A general model for carbon isotopes in red-lineage phytoplankton: Interplay between unidirectional processes and fractionation by RubisCO. *Geochim. Cosmochim. Acta* **265**, 163–181 (2019).
38. E. A. Laws *et al.*, Controls on the molecular distribution and carbon isotopic composition of alkenones in certain haptophyte algae. *Geochem. Geophys. Geosyst.* **2**, 1006–1031 (2001).
39. K. L. Terry, J. Hirata, E. A. Laws, Light-, nitrogen-, and phosphorus-limited growth of Phaeodactylum tricornutum Bohlin Strain TFX-1: Chemical composition, carbon partitioning, and the diel periodicity of physiological processes. *J. Exp. Mar. Biol. Ecol.* **86**, 85–100 (1985).
40. B. N. Popp, F. G. Prahl, R. J. Wallsgrove, J. Tanimoto, Seasonal patterns of alkenone production in the subtropical oligotrophic North Pacific. *Paleoceanography* **21**, PA1004 (2006).
41. D. K. Steinberg *et al.*, Overview of the US JGOFS Bermuda Atlantic Time-series Study (BATS): A decade-scale look at ocean biology and biogeochemistry. *Deep Sea Res. Part II: Top. Stud. Oceanogr.* **48**, 1405–1447 (2001).
42. M. D. DuRand, R. J. Olson, S. W. Chisholm, Phytoplankton population dynamics at the Bermuda Atlantic Time-series station in the Sargasso Sea. *Deep Sea Res. Part II: Top. Stud. Oceanogr.* **48**, 1983–2003 (2001).
43. A. T. Haidar, H. R. Thierstein, Coccolithophore dynamics off Bermuda (N. Atlantic). *Deep Sea Res. Part II: Top. Stud. Oceanogr.* **48**, 1925–1956 (2001).
44. E. A. Laws, B. N. Popp, N. Cassar, J. Tanimoto, 13C discrimination patterns in oceanic phytoplankton: Likely influence of CO2 concentrating mechanisms, and implications for palaeoreconstructions. *Funct. Plant Biol.* **29**, 323–333 (2002).
45. J. A. Raven, L. A. Ball, J. Beardall, M. Giordano, S. C. Maberly, Algae lacking carbon-concentrating mechanisms. *Can. J. Bot.* **83**, 879–890 (2005).
46. W. G. Mook, J. C. Bommerson, W. H. Staverman, Carbon isotope fractionation between dissolved bicarbonate and gaseous carbon dioxide. *Earth Planet. Sci. Lett.* **22**, 169–176 (1974).
47. U. Riebesell, D. Wolf-Gladrow, Growth limits on phytoplankton. *Nature* **373**, 28 (1995).
48. Q. Liu *et al.*, Temperature is a better predictor of stable carbon isotopic compositions in marine particulates than dissolved CO2 concentration. *Commun. Earth Environ.* **3**, 303 (2022).
49. I. Kriest, A. Oschlies, Modelling the effect of cell-size-dependent nutrient uptake and exudation on phytoplankton size spectra. *Deep Sea Res. Part I: Oceanogr. Res. Pap.* **54**, 1593–1618 (2007).
50. D. N. Rao, M. Chopra, G. R. Rajula, D. S. L. Durgadevi, V. V. S. S. Sarma, Release of significant fraction of primary production as dissolved organic carbon in the Bay of Bengal. *Deep Sea Res. Part I: Oceanogr. Res. Pap.* **168**, 103445 (2021).
51. A. W. A. Jeffrey, R. C. Pflaum, J. M. Brooks, W. M. Sackett, Vertical trends in particulate organic carbon 13C:12C ratios in the upper water column. *Deep Sea Res. Part A. Oceanogr. Res. Pap.* **30**, 971–983 (1983).
52. T. C. Malone, S. E. Pike, D. J. Conley, Transient variations in phytoplankton productivity at the JGOFS Bermuda time series station. *Deep Sea Res. Part I: Oceanogr. Res. Pap.* **40**, 903–924 (1993).
53. K. Gundersen, K. M. Orcutt, D. A. Purdie, A. F. Michaels, A. H. Knap, Particulate organic carbon mass distribution at the Bermuda Atlantic Time-series Study (BATS) site. *Deep Sea Res. Part II: Top. Stud. Oceanogr.* **48**, 1697–1718 (2001).
54. Y. T. Yamaguchi *et al.*, Fractionation of nitrogen isotopes during amino acid metabolism in heterotrophic and chemolithoautotrophic microbes across Eukarya, Bacteria, and Archaea: Effects of nitrogen sources and metabolic pathways. *Org. Geochem.* **111**, 101–112 (2017).
55. H. G. Close *et al.*, Export of submicron particulate organic matter to mesopelagic depth in an oligotrophic gyre. *Proc. Natl. Acad. Sci. U.S.A.* **110**, 12565–12570 (2013).
56. C. A. Durkin, M. L. Estapa, K. O. Buesseler, Observations of carbon export by small sinking particles in the upper mesopelagic. *Mar. Chem.* **175**, 72–81 (2015).
57. P. W. Boyd, H. Claustre, M. Levy, D. A. Siegel, T. Weber, Multi-faceted particle pumps drive carbon sequestration in the ocean. *Nature* **568**, 327–335 (2019).
58. F. Pollehne, B. Klein, B. Zeitzschel, Low light adaptation and export production in the deep chlorophyll maximum layer in the northern Indian Ocean. *Deep Sea Res. Part II: Top. Stud. Oceanogr.* **40**, 737–752 (1993).
59. P. B. Ortner, P. Wiebe, J. L. Cox, Relationships between oceanic epizooplankton distributions and the seasonal deep chlorophyll maximum in the northwestern Atlantic Ocean. *J. Mar. Res.* **38**, 507–531 (1980).
60. J. S. Sinninghe Damsté, M. M. M. Kuypers, R. D. Pancost, S. Schouten, The carbon isotopic response of algae, (cyano)bacteria, archaea and higher plants to the late Cenomanian perturbation of the global carbon cycle: Insights from biomarkers in black shales from the Cape Verde Basin (DSDP Site 367). *Org. Geochem.* **39**, 1703–1718 (2008).
61. K. L. Bice *et al.*, A multiple proxy and model study of Cretaceous upper ocean temperatures and atmospheric CO2 concentrations. *Paleoceanography* **21**, PA2002 (2006).
62. B. Matthews, A. Mazumder, Habitat specialization and the exploitation of allochthonous carbon by zooplankton. *Ecology* **87**, 2800–2812 (2006).
63. A. F. Michaels, A. H. Knap, Overview of the U.S. JGOFS Bermuda Atlantic time-series study and the hydrostation S program. *Deep Sea Res. Part II: Top. Stud. Oceanogr.* **43**, 157–198 (1996).
64. J. Sprintall, M. Tomczak, Evidence of the barrier layer in the surface layer of the tropics. *J. Geophys. Res.: Oceans* **97**, 7305–7316 (1992).
65. E. G. Bligh, W. J. Dyer, A rapid method of total lipid extraction and purification. *Can. J. Biochem. Physiol.* **37**, 911–917 (1959).
66. H. F. Sturt, R. E. Summons, K. Smith, M. Elvert, K.-U. Hinrichs, Intact polar membrane lipids in prokaryotes and sediments deciphered by high-performance liquid chromatography/electrospray ionization multistage mass spectrometry–New biomarkers for biogeochemistry and microbial ecology. *Rapid Commun. Mass Spectrom.* **18**, 617–628 (2004).
67. T. P. Bastow, B. G. K. van Aarssen, D. Lang, Rapid small-scale separation of saturate, aromatic and polar components in petroleum. *Org. Geochem.* **38**, 1235–1250 (2007).
68. H. G. Close, S. G. Wakeham, A. Pearson, Lipid and 13C signatures of submicron and suspended particulate organic matter in the Eastern Tropical North Pacific: Implications for the contribution of Bacteria. Deep Sea Res. Part I: Oceanogr. *Res. Pap.* **85**, 15–34 (2014).
69. C. C. S. Hannides, B. N. Popp, C. A. Choy, J. C. Drazen, Midwater zooplankton and suspended particle dynamics in the North Pacific Subtropical Gyre: A stable isotope perspective. *Limnol. Oceanogr.* **58**, 1931–1946 (2013).
70. Y. Chikaraishi *et al.*, Determination of aquatic food-web structure based on compound-specific nitrogen isotopic composition of amino acids: Trophic level estimation by amino acid δ^{15}N. *Limnol. Oceanogr. Methods* **7**, 740–750 (2009).
71. C. L. Jarman *et al.*, Diet of the prehistoric population of Rapa Nui (Easter Island, Chile) shows environmental adaptation and resilience. *Am. J. Phys. Anthropol.* **164**, 343–361 (2017).
72. P. G. Verity *et al.*, Relationships between cell volume and the carbon and nitrogen content of marine photosynthetic nanoplankton. *Limnol. Oceanogr.* **37**, 1434–1446 (1992).
73. A. Z. Worden, J. K. Nolan, B. Palenik, Assessing the dynamics and ecology of marine picophytoplankton: The importance of the eukaryotic component. *Limnol. Oceanogr.* **49**, 168–179 (2004).
74. E. Lessard, M. Murrell, Microzooplankton herbivory and phytoplankton growth in the northwestern Sargasso Sea. *Aquat. Microb. Ecol.* **16**, 173–188 (1998).
75. S. Van Heuven, D. Pierrot, J. W. B. Rae, E. Lewis, D. W. R. Wallace, MATLAB program developed for CO2 system calculations. ORNL/CDIAC-105b (2011), 10.3334/CDIAC/OTG.CO2SYS_MATLAB_V1.1 (14 June 2022).
76. C. Carlson, S. Giovannoni, S. Liu, E. Halewood, Project: Bermuda Institute of Ocean Sciences Simons Collaboration on Ocean Processes and Ecology. Biological and Chemical Oceanography Data Management Office (BCO-DMO). https://www.bco-dmo.org/project/826178. Deposited 14 June 2022.